Theor Chem Acc (2010) 127:551–560
DOI 10.1007/s00214-010-0746-2

REGULAR ARTICLE

Theoretical studies of the reactions of Cl atoms with $CF_3CH_2OCH_nF_{(3-n)}$ (n = 1, 2, 3)

Hui Zhang · Cheng-yang Liu · Gui-ling Zhang · Wen-jie Hou · Miao Sun · Bo Liu · Ze-sheng Li

Received: 16 October 2009 / Accepted: 11 March 2010 / Published online: 6 April 2010

Abstract This paper presents the theoretical studies of the reactions of Cl atoms with $CF_3CH_2OCH_3$, $CF_3CH_2OCH_2F$ and $CF_3CH_2OCHF_2$ using an ab initio direct dynamics theory. The geometries and vibrational frequencies of the reactants, complexes, transition states and products are calculated at the MP2/6-31+(d,p) level. The minimum energy path is also calculated at same level. The MC-QCISD method is carried out for further refining the energetic information. The rate constants are evaluated with the canonical variational transition state theory (CVT) and CVT with small curvature tunneling contributions in the temperature range 200–1,500 K. The results are in good agreement with experimental values.

Keywords Ab initio · HFEs · CVT · Rate constants

1 Introduction

The depletion of atmospheric ozone layer directly relates to the characteristics of global climate and environmental quality. The magnificent and victorious activities had been launched throughout the world for protecting ozone layer. Governments of all countries have been convinced of the importance of this problem; thus, a series of international activities and treaties have been produced. The researches indicate that the main reasons for ozone depletion are chlorine and bromine, which are emitted from the chlorofluorocarbons (CFCs), and these atoms can deplete stratospheric ozone [1]. A number of compounds such as hydrofluoroethers (HFEs), which contain no chlorine and bromine atoms, are being considered to substitute the chlorofluorocarbons. But the C–F bond in HFES can cause green house effect by introducing the ether linkage -O- which has greater reactivity in the troposphere [2]. So it is necessary to investigate the activity of HFEs in the atmosphere. Cl atoms may be a significant part of the degradation of HFEs because of its higher reactivity [3]. This paper presents a systematic theoretical investigation of the reactions $Cl + CF_3CH_2OCH_3$ (R_1), $Cl + CF_3CH_2OCH_2F$ (R_2) and $Cl + CF_3CH_2OCHF_2$ (R_3).

The dual-level direct dynamics method is carried out to investigate the mechanisms of the title reactions. There are two H-abstraction channels for each reaction and performed as follows:

Electronic supplementary material The online version of this article (doi:10.1007/s00214-010-0746-2) contains supplementary material, which is available to authorized users.

H. Zhang (✉) · C. Liu · G. Zhang · W. Hou · M. Sun · B. Liu
College of Chemical and Environmental Engineering,
Harbin University of Science and Technology,
150080 Harbin, People's Republic of China
e-mail: hust_zhanghui11@hotmail.com

Z. Li (✉)
Academy of Fundamental and Interdisciplinary Sciences,
Department of Chemistry,
Harbin Institute of Technology,
150080 Harbin, People's Republic of China
e-mail: zeshengli@hit.edu.cn

Z. Li
School of Sciences, Beijing Institute of Technology,
100081 Beijing, People's Republic of China

$$CF_3CH_2OCH_3 + Cl \xrightarrow[k_{1a}]{} CF_3CHOCH_3 + HCl \quad (R_{1a})$$

$$CF_3CH_2OCH_3 + Cl \xrightarrow[k_{1b}]{} CF_3CH_2OCH_2 + HCl \quad (R_{1b})$$

$$CF_3CH_2OCH_2F + Cl \xrightarrow[k_{2a}]{} CF_3CHOCH_2F + HCl \quad (R_{2a})$$

$$CF_3CH_2OCH_2F + Cl \xrightarrow[k_{2b}]{} CF_3CH_2OCHF + HCl \quad (R_{2b})$$

$$CF_3CH_2OCHF_2 + Cl \xrightarrow[k_{3a}]{} CF_3CHOCHF_2 + HCl \quad (R_{3a})$$

$$CF_3CH_2OCHF_2 + Cl \xrightarrow[k_{3b}]{} CF_3CH_2OCF_2 + HCl \quad (R_{3b})$$

For the reaction R_1, two experimental investigations were reported by Oyaro et al. [4] at 298 K and Kyriakos et al. [5] in the temperature range of 273–363 K. Many studies have focused on the reaction R_3, and five experimental investigations [4–8] and a theoretical study [9] have been reported in the temperature range of 273–363 and 200–2,000 K, respectively. The experimental values of R_1, R_3 are $(1.8 \pm 0.9) \times 10^{-11}$ and $(1.5 \pm 0.4) \times 10^{-14}$, respectively, at 298 K. As far as we know, no theoretical investigation has been reported about R_1 and R_2.

There are other reaction channels for R_1, R_2 and R_3:

$$CF_3CH_2OCH_3 + Cl \rightarrow CF_3CH_2O + CH_3Cl \quad (R_{1c})$$

$$CF_3CH_2OCH_3 + Cl \rightarrow CH_3OCH_2 + CF_3Cl \quad (R_{1d})$$

$$CF_3CH_2OCH_2F + Cl \rightarrow CF_3CH_2O + CH_2FCl \quad (R_{2c})$$

$$CF_3CH_2OCH_2F + Cl \rightarrow CH_2OCH_2F + CF_3Cl \quad (R_{2d})$$

$$CF_3CH_2OCHF_2 + Cl \rightarrow CF_3CH_2O + CHF_2Cl \quad (R_{3c})$$

$$CF_3CH_2OCHF_2 + Cl \rightarrow CHF_2OCH_2 + CF_3Cl \quad (R_{3d})$$

The experiment investigated is mostly in the temperature range of 273–363 K. In this paper, theoretical study gives a temperature range 200–1,500 K and evaluates the rate constants of R_1, R_2 and R_3 studied by direct dynamic method and compared with the experiment values. And the F replacement effect has been discussed for the H-abstraction channel on the rate constants of this class of hydrogen abstraction reactions.

The dual-level direct dynamics method proposed by Truhlar and co-worker [10–12] is carried out to investigate the kinetic nature of the title reactions. And the potential energy surface information is obtained directly from electronic structure calculations. Subsequently, by means of POLYRATE 9.1 program [13], the rate constants calculated using the CVT and CVT/SCT method proposed by Truhlar et al. [14, 15].

2 Computational method

In the present paper, the optimized geometries and vibrational frequencies of reactants, complexes, transitions states and products are calculated by MP2 (restricted or unrestricted second-order Møller–Plesset perturbation theory) [16–18] method with 6-31+G(d,p) basis set. With the same method and basis set, the minimum energy path (MEP) [19–21] are obtained by intrinsic reaction coordinate (IRC) theory [22–24] with a gradient step size of 0.05 $(amu)^{1/2}$ bohr, the harmonic vibrational frequencies as well as the force constant matrices of the selected points (40 points were computed on each side of the saddle points in the IRC calculations and 16 non-stationary points were selected for the CVT calculations) along the IRC are also calculated at the MP2/6-31+(d,p) level. The MC-QCISD method (multi-coefficient correlation method based on quadratic configuration interaction with single and double excitations proposed by Fast and Truhlar) [25] is employed to refine the energy based on the MP2/6-31+G(d,p) geometries. All of the works are carried out by the GAUSSIAN03 program package [26].

Ab initio calculation allowed us to calculate the rate constants of all the reaction channels. The canonical variational theory (CVT) [14, 15] based on the idea of varying the dividing surface along a reference path to minimize the rate constant is given as follows:

$$k^{CVT}(T) = \min_s k^{GT}(T, s) \quad (1)$$

where

$$k^{GT}(T, s) = \frac{\sigma k_B T Q^{GT}(T, s)}{h\Phi^R(T)} e^{-V_{MEP}(s)/k_B T} \quad (2)$$

In which, $k^{GT}(T, s)$ is the rate constant at the dividing surfaces, and σ is the symmetry factor accounting for the possibility of more than one symmetry-related reaction path, h is Plank's constant, k_B is Boltzman's constant, and $Q^{GT}(T, s)$ is the partition function of a generalized transition state at s with a local zero of energy at $V_{MEP}(s)$ and with all rotational symmetry numbers set to unity. $Q^R(T)$ is the reactant partition function per unit volume excluding symmetry numbers for rotation. Considered the tunneling reaction, the traditional transition state theory (TST), CVT and CVT/SCT are carried out for calculating the rate constants [27–29]. The hindered-rotor approximation of Chuang and Truhlar [30, 31] was used for calculating the partition functions of all the modes associated with the torsion. The curvature components are calculated using a quadratic fit to obtain the derivative of the gradient with respect to the reaction coordinate. All the kinetic calculations have been carried out with the POLYRATE 9.1 program package [13].

3 Results and discussion

3.1 Stationary points

In Fig. 1, all the optimized geometric parameters of the stationary points of several products with the available

experimental values (given in the parentheses) and transition states which were calculated at the MP2/6-31+G(d,p) [16–18] level are presented. And the reactants, complexes and products which were calculated at the same level are presented in Fig. S1 as supporting information. From Fig. 1, we note that the optimized geometric parameters of HCl, CH_3Cl, CH_2FCl and CHF_2Cl are reasonably consistent with the corresponding experimental values [32, 33]. For the H-abstraction transition states (TS_{1a}, TS_{1b} and TS_{2b}), the length of the breaking C–H bonds are enlarged by 14.6, 17.4 and 13.8%, respectively, compared to the equilibrium bonds length of $CF_3CH_2OCH_3$ and $CF_3CH_2OCH_2F$. And the forming bond length (TS_{1a}, TS_{1b} and TS_{2b}) of H–Cl increased by 22.8, 20.7 and 23.7% over the regular bond lengths of HCl. So the elongation of the forming bond is larger than the breaking bond. In the transition states TS_{1d}, TS_{2d} and TS_{3d}, the breaking C–C bonds are larger than the equilibrium bond length of $CF_3CH_2OCH_3$, $CF_3CH_2OCH_2F$ and $CF_3CH_2OCHF_2$ by 26.3, 27.7 and 26.9%, respectively, the forming C–Cl bond length is stretched by 59.9, 59.7 and 59.6% compared with the bond length of CF_3Cl.

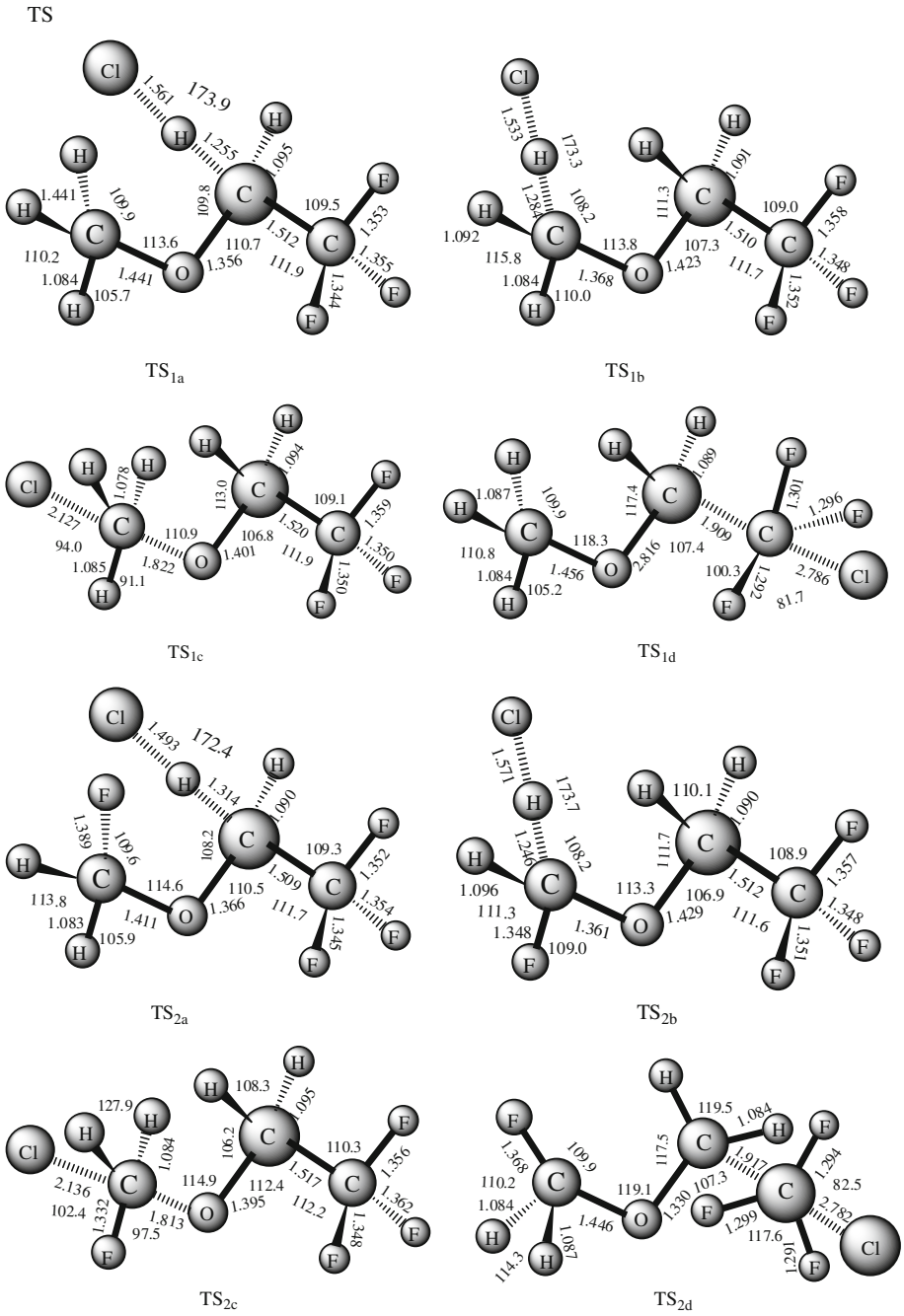

Fig. 1 Optimized geometries of the transitions states and several products at the MP2/6-31+G(d,p) level

Fig. 1 continued

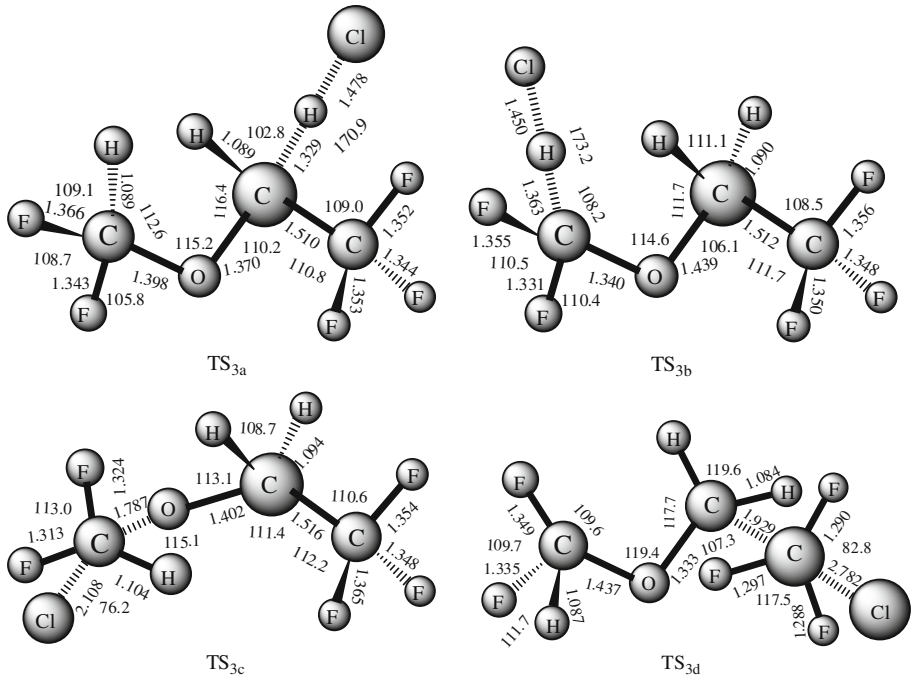

Products

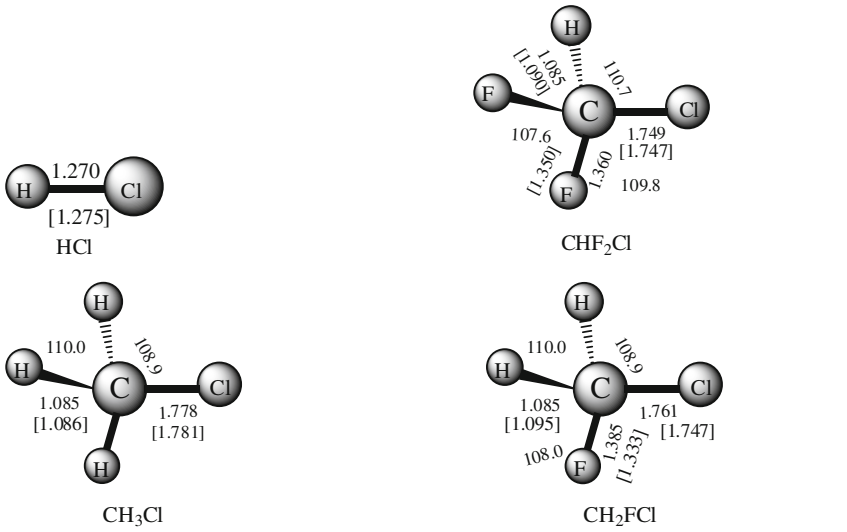

While the transition states TS_{2a}, TS_{3a} and TS_{3b} present that the breaking C–H bond length is enlarged by 20.0, 21.7 and 24.9%, and the forming H–Cl bond length increased by 17.2, 16.4 and 14.2% over the equilibrium bond length, respectively. Meanwhile, in the transition states TS_{1c}, TS_{2c} and TS_{3c}, the breaking C–O bond length is elongated by 27.8, 29.7 and 30.4%, and the forming C–Cl bond length are stretched by 19.7, 21.3 and 20.5% compared with the regular correspond bond length, respectively. The elongation of the breaking bonds for TS_{2a}, TS_{3a} and TS_{3b} are larger than the forming bonds, which indicates that both of them are product-like and will proceed via "late" transition states.

The harmonic vibrational frequencies of all the stationary points of transition states which calculated at the MP2/6-31+G(d,p) level are given in Table S1, and the values of reactants, complexes and products are listed in Table S2 as supporting information. From the tables, we can see that the frequencies are in agreement with the experimental values [34–36] with the largest deviation within 7%. And all the transition states structures are confirmed by normal-mode analysis to have one and only one imaginary frequency corresponding to the stretching modes of the coupling breaking and forming bond. The values of these imaginary frequencies (cm^{-1}) are 884 *i* for TS_{1a}, 835 *i* for TS_{1b}, 1,606 *i* for TS_{1c}, 479 *i* for TS_{1d}, 1,223

i for TS_{2a}, 705 *i* for TS_{2b}, 1,771 *i* for TS_{2c}, 826 *i* for TS_{2d}, 1,245 *i* for TS_{3a}, 1,168 *i* for TS_{3b}, 1,825 *i* for TS_{3c}, 1,314 *i* for TS_{3d}. And the reactants, products and complexes possess only real frequencies.

3.2 Energetics

The reaction enthalpies (ΔH^0_{298}) and the potential barrier heights (ΔE^{TS}) with zero-point energy (ZPE) corrections for all the reaction channels calculated at the MC-QCISD//MP2/6-31+G(d,p) level, and the corresponding data are listed in Table 1, As listed in Table 1, all of the H-abstraction reaction channels are exothermic, and the value of the channel R_{1a} is the lowest comparing with the corresponding others ones, similar features can be drawn from R_{2a} and R_{3a} channels. The values of enthalpies are −8.68, −10.33 and −7.02 kcal/mol for R_{1a}, R_{2a} and R_{3a}, respectively. The values of the three channels (R_{1b}, R_{2b} and R_{3b}) are −7.02, −7.04 and −1.27 kcal/mol, respectively. Contrarily, the reaction channels R_{1c}, R_{1d}, R_{2c}, R_{2d}, R_{3c} and R_{3d} of the reactions are endothermic, and the values of enthalpies can be seen from Table 1. Relative energies of the stationary points in terms of enthalpy and Gibbs free energy also listed in Table S3 as supporting information.

A schematic potential energy diagram of the reactions R_1, R_2 and R_3 with ZPE corrections obtained at the MC-QCISD//MP2/6-31+G(d,p) level are plotted in Figs. 2, 3 and 4. Figure 2 indicates that the reaction channel R_{1b} has the lowest barrier height (−5.58 kcal/mol), and the values of R_{1a}, R_{1c} and R_{1d} are about 1.26, 43.94 and 78.45 kcal/mol higher than that of R_{1b}, respectively. Consequently, the reaction channel R_{1b} is more kinetically favorable than the other three channels of R_1. As shown in Fig. 3, the reaction channels R_{2b}, R_{2c} and R_{2d} have higher barrier height about 1.38, 46.23 and 85.18 kcal/mol than R_{2a} (−5.86 kcal/mol). As a result, the channel R_{2a} may be the dominant reaction pathway on the rate constant. Meanwhile, similar conclusion can be obtained from Fig. 4. Figure 4 shows that the barrier height value of R_{3a} is −0.32 kcal/mol, and R_{3b} (0.91 kcal/mol), R_{3c} (55.81 kcal/mol) and R_{3d} (82.31 kcal/mol) are about 1.23, 56.13 and 82.63 kcal/mol higher than R_{3a}, respectively. Thus, for the reaction R_3, the channel R_{3a} is more favorable than R_{3b}, R_{3c} and R_{3d}. For all the reaction channels, the R_{2a} has the lowest barrier height, so the R_{2a} channel is the most kinetically favorable and it is expected to have the largest rate constant.

For the reaction R_1, the H-abstraction of the $–CH_3$ group is more likely to occur than the others, and the H-abstraction of the $–CH_2–$ group is more favorable for R_2 and R_3. Furthermore, the H-abstraction barrier height of R_3 is higher than R_2 one, this phenomena may be because the changes in electron density distribution, because the $–CHF_2$ group is more electron-withdrawing than $–CH_2F$ one.

In order to determine which of the channels is most likely to occur, the bond dissociation energies (BDEs) of the three reactants are calculated at the MC-QCISD//MP2/6-31+G(d,p) level and the values are listed in Table 2 together with available experimental data [5], and the calculated values are in good agreement with the corresponding experimental data [5]. From Table 2, we can see that the C–H bond of $–CH_2–$ group of $CF_3CH_2OCFH_2$ has the lowest BDEs value (92.66 kcal/mol), which is expect has the fastest rate constant, the result is line with the potential energy diagram above-mentioned. But for the $CF_3CH_2OCH_3$ molecule, as listed in Table 2, the C–H BDEs of $–CH_2–$ group is lower than that of $–CH_3$ group, which is indicating that, the H-abstraction of $–CH_2–$ is more likely to occur. This conclusion is inconsistent with the description of Fig. 2. This inconsistent has been explained by Kyriakos et al. [5] in 1998, they think that the H-abstraction of the methyl should lead to a higher pre-exponential factor considering the higher entropy of the corresponding transition state due to the larger external

Table 1 The reaction enthalpies at 298 K (ΔH^0_{298}) and the barrier height ΔE (kcal/mol) for each of the reactions at the MC-QCISD//MP2/6-31+G(d,p) level

Reaction	ΔH^0_{298}	ΔE
$CF_3CH_2OCH_3 + Cl \rightarrow CF_3CHOCH_3 + HCl$	−8.68	−4.32
$CF_3CH_2OCH_3 + Cl \rightarrow CF_3CH_2OCH_2 + HCl$	−7.02	−5.58
$CF_3CH_2OCH_3 + Cl \rightarrow CF_3CH_2O + CH_3Cl$	7.64	38.36
$CF_3CH_2OCH_3 + Cl \rightarrow CH_3OCH_2 + CF_3Cl$	8.51	72.87
$CF_3CH_2OCH_2F + Cl \rightarrow CF_3CHOCH_2F + HCl$	−10.33	−5.86
$CF_3CH_2OCH_2F + Cl \rightarrow CF_3CH_2OCHF + HCl$	−7.02	−4.48
$CF_3CH_2OCH_2F + Cl \rightarrow CF_3CH_2O + CH_2FCl$	11.80	40.37
$CF_3CH_2OCH_2F + Cl \rightarrow CH_2OCH_2F + CF_3Cl$	10.58	79.32
$CF_3CH_2OCHF_2 + Cl \rightarrow CF_3CHOCHF_2 + HCl$	−5.32	−0.32
$CF_3CH_2OCHF_2 + Cl \rightarrow CF_3CH_2OCF_2 + HCl$	−1.27	0.91
$CF_3CH_2OCHF_2 + Cl \rightarrow CF_3CH_2O + CHF_2Cl$	19.37	55.81
$CF_3CH_2OCHF_2 + Cl \rightarrow CHF_2OCH_2 + CF_3Cl$	9.49	82.31

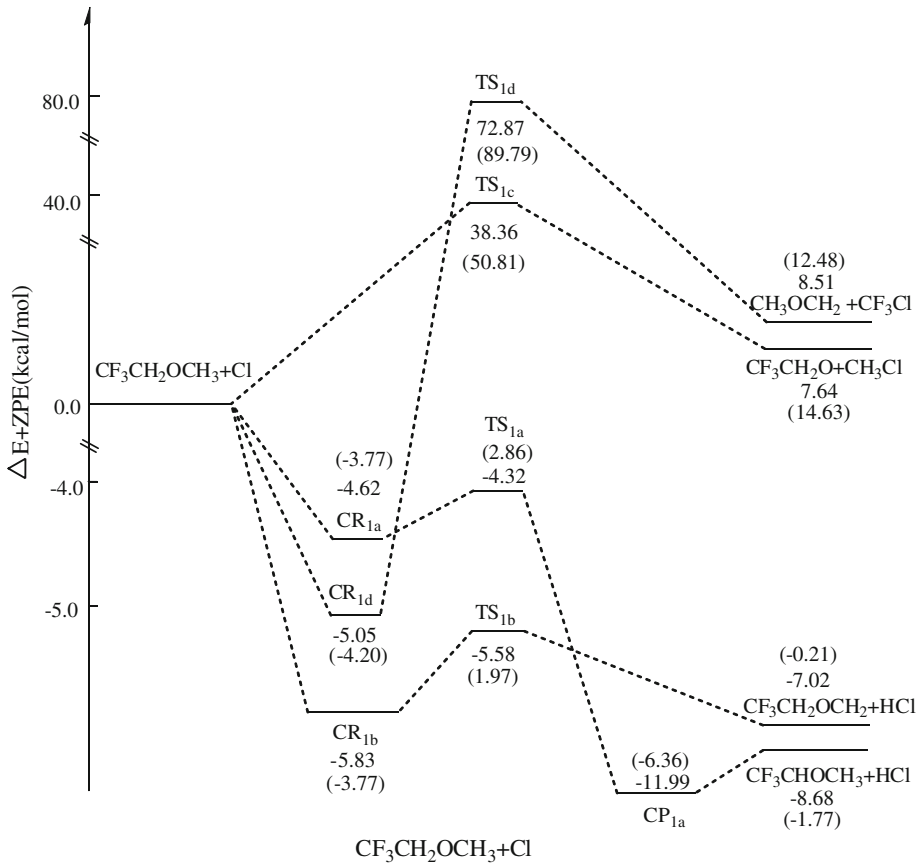

Fig. 2 Schematic potential energy surface for the reaction R_1. Relative energies (in kcal/mol) are calculated at the MC-QCISD//MP2/6-31+G(d,p)+ZPE level. The values in *parentheses* are calculated at the MP2/6-31+G(d,p)+ZPE level

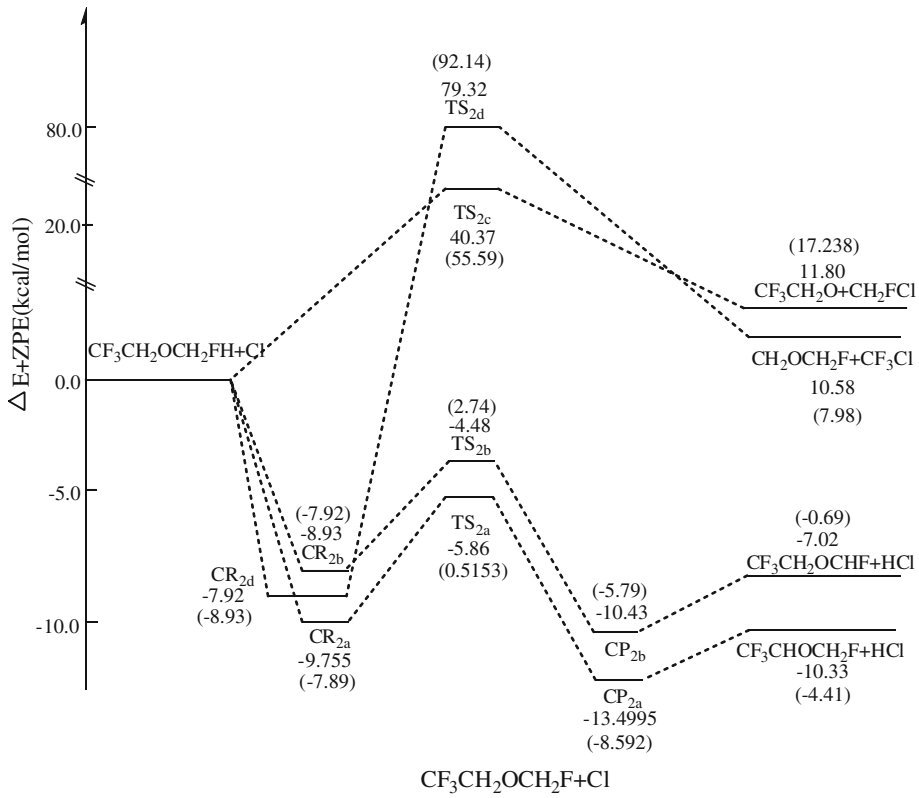

Fig. 3 Schematic potential energy surface for the reaction R_2. Relative energies (in kcal/mol) are calculated at the MC-QCISD//MP2/6-31+G(d,p)+ZPE level. The values in *parentheses* are calculated at the MP2/6-31+G(d,p)+ZPE level

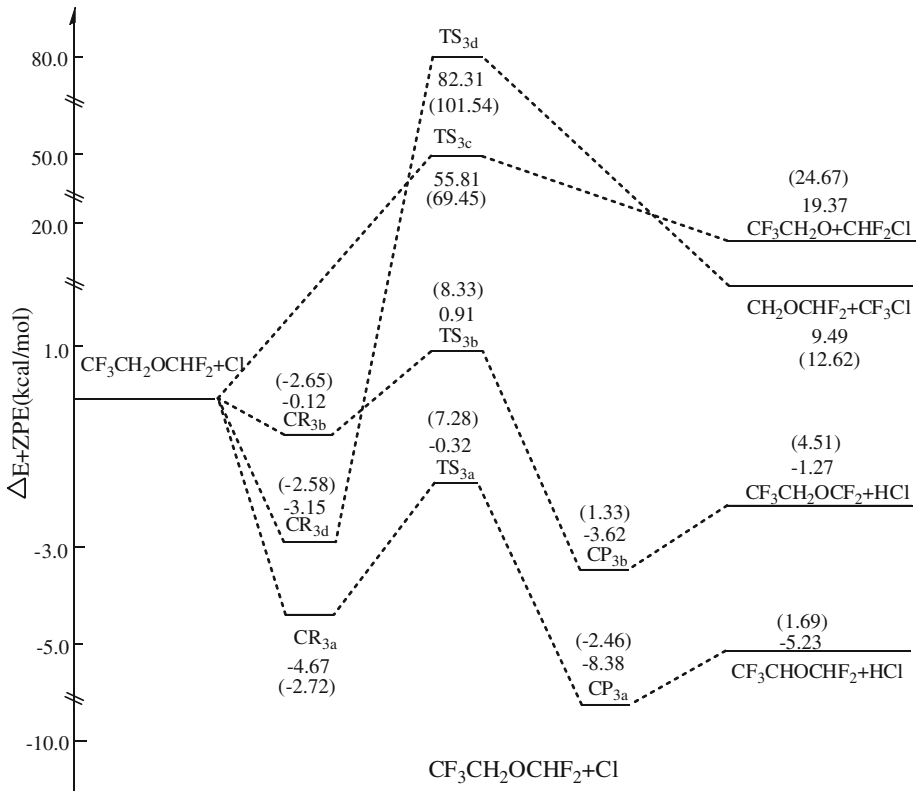

Fig. 4 Schematic potential energy surface for the reaction R_3. Relative energies (in kcal/mol) are calculated at the MC-QCISD//MP2/6-31+G(d,p)+ZPE level. The values in *parentheses* are calculated at the MP2/6-31+G(d,p)+ZPE level

moments of inertia of $[CF_3CH_2OCH_2\cdots H\cdots Cl]^{\neq}$ compared to $[CF_3CH(\cdots H\cdots Cl)OCH_3]^{\neq}$ transition state configuration. So the H-abstraction of the methyl group is more likely to occur for the reaction R_1. Due to the very high barrier height, the rate constants of R_{1c}, R_{1d}, R_{2c}, R_{2d}, R_{3c} and R_{3d} is negligible. Thus, in the present work, we calculate the rate constant for the reaction channels R_{1a}, R_{1b}, R_{2a}, R_{2b}, R_{3a} and R_{3b} in the following studies.

3.3 Rate constants

The rate constants of the reactions $Cl + CF_3CH_2OCH_3$, $Cl + CF_3CH_2OCH_2F$ and $Cl + CF_3CH_2OCHF_2$ are obtained by employing the dual-level dynamics [14, 15] at the MC-QCISD//MP2/6-31+G(d,p) level. The conventional transition state theory (TST), CVT and CVT/SCT of reaction channels R_{1a}, R_{1b}, R_{2a}, R_{2b}, R_{3a} and R_{3b} are carried out in a wide temperature range from 200 to 1,500 K. The CVT/SCT rate constant curves of each reaction channels are plotted in Fig. 5.

The calculated total CVT/SCT rate constants of R_1, R_2, R_3, and the available experimental values are listed in Table 3, and the values of TST, CVT, ZCT and SCT for each channel are listed in Table S4 as supporting information. We can see from the table that the rate constants calculated at 298 K are 2.55×10^{-11} and 3.99×10^{-14} cm^3 $molecule^{-1}$ s^{-1}, which are in good agreement with the experimental values, $(1.8 \pm 0.9) \times 10^{-11}$ and $(1.5 \pm 0.4) \times 10^{-14}$ cm^3 $molecule^{-1}$ s^{-1} of R_1 and R_3, respectively, obtained by Oyaro et al. [4]. Furthermore, Kyriakos et al. [5] have also obtained the rate constants of R_1 ($(2.31 \pm 0.1) \times 10^{-11}$ cm^3 $molecule^{-1}$ s^{-1}) and R_3((3.11

Table 2 Bond dissociation energies (kcal/mol) for all the reaction channels at the MP2/6-31+G(d,p) and MC-QCISD//MP2/6-31+G(d,p) level

Bond	MP2/6-31+G(d,p)	MC-QCISD	Expt.
C–H			
$CF_3(C–H)HOCH_3$	91.22	95.29	95.22[a]
$CF_3CH_2O(C–H)H_2$	92.79	96.95	97.13[a]
$CF_3(C–H)HOCH_2F$	88.60	92.66	
$CF_3CH_2O(C–H)HF$	92.31	96.97	
$CF_3(C–H)HOCHF_2$	94.70	98.76	98.09[a]
$CF_3CH_2O(C–H)F_2$	97.52	102.72	102.39[a]
C–O			
$CF_3CH_2O–CH_3$	91.33	90.62	
$CF_3CH_2O–CH_2F$	97.20	96.49	
$CF_3CH_2O–CHF_2$	106.56	105.58	
C–C	6		
$F_3C–CH_2OCH_3$	95.47	95.58	
$F_3C–CH_2OCH_2F$	90.91	92.64	
$F_3C–CH_2OCHF_2$	95.62	96.56	

[a] Ref. [5]

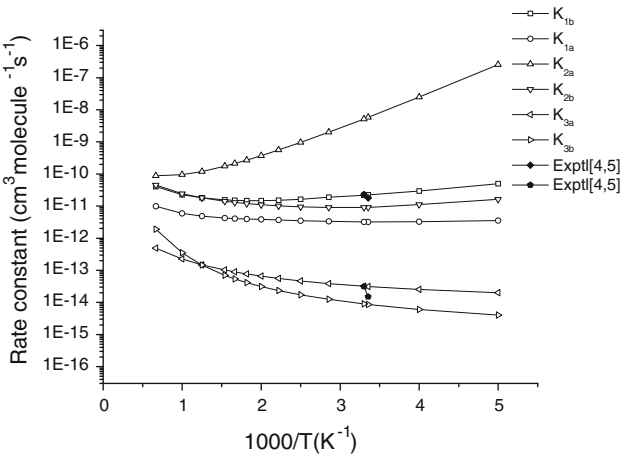

Fig. 5 The CVT/SCT rate constants calculated at the MC-QCISD//MP2/6-31+G(d,p) level for all the H-abstraction reaction channels (in cm^3 $molecule^{-1}$ s^{-1}), vs. 1,000/*T* between 200 and 1,500 K, together with the experimental value

Table 3 The total CVT/SCT rate constants calculated at the MC-QCISD//MP2/6-31+G(d,p) level for three reactions, R_1, R_2 and R_3 between 200 and 1,500 K(cm^3 $molecule^{-1}$ s^{-1})

T(K)	k_1	k_2	k_3	Expt.	
				k_1	k_2
200	5.36 E-11	2.57 E-7	2.40 E-14		
250	3.26 E-11	2.49 E-8	3.13 E-14		
298	2.55 E-11	5.85 E-9	3.99 E-14	(1.8 ± 0.9)[a] E-11	(1.5 ± 0.4)[a] E-14
303	2.51 E-11	5.18 E-9	4.08 E-14	(2.31 ± 0.1)[b] E-11	(3.11 ± 0.14)[b] E-14
350	2.22 E-11	2.01 E-9	5.11 E-14		
400	1.98 E-11	9.63 E-10	6.40 E-14		
450	1.89 E-11	5.71 E-10	7.93 E-14		
500	1.87 E-11	3.84 E-10	9.71 E-14		
550	1.88 E-11	2.84 E-10	1.18 E-13		
600	1.92 E-11	2.26 E-10	1.42 E-13		
650	1.98 E-11	1.89 E-10	1.71 E-13		
800	2.29 E-11	1.38 E-10	2.94 E-13		
1,000	2.88 E-11	1.20 E-10	5.79 E-13		
1,500	5.02 E-11	1.33 E-10	2.39 E-12		

[a] Ref. [4], [b] Ref. [5]

± 0.14) × 10^{-14} cm^3 $molecule^{-1}$ s^{-1}) at 303 K, and the values we calculated at 303 K are 2.51 × 10^{-11} and 4.08 × 10^{-14} cm^3 $molecule^{-1}$ s^{-1} for the reactions R_1 and R_3, respectively. From Fig. 5, we can see that the reaction channels R_{1b}, R_{2a} and R_{3a} are dominate channels for R_1, R_2 and R_3, respectively, in the temperature range of 200–1,500 K. And the channel R_{2a} has an obviously negative temperature dependence whose rate constant is decreasing with the temperature increasing.

The rate constants TST, CVT and CVT/SCT of R_{2a} and R_{3b} are plotted in Figs. 6, 7. As shown in Fig. 6, the three curves are almost overlapped, and it indicates that the variational effect and small curvature effect could be negligible on R_{2a} in the whole temperature range. And we can see from Fig. 7 that the CVT/SCT rate constants are much larger than that of the CVT ones at the lower temperature range, but the three curves are asymptotic in the higher temperatures, the ratio values we obtained of $k_{CVT/SCT}/k_{CVT}$ are 7.22 × 10^6, 47.49 and 2.19 for the channel R_{3b}, at the temperatures 200, 500 and 1,000 K, respectively. So we can conclude that the small curvature effect plays an important role in lower temperature range. And similar conclusions can be obtained for the others reaction channels R_{1a}, R_{1b}, R_{2b}, R_{3a}.

The branching ratios of R_1, R_2 and R_3 are calculated, and the ratio curves of R_2 are presented in Fig. 8. The ratios of $k_{2a}/k_{(2a+2b)}$ are 0.99, 0.94 and 0.66 at 200, 600 and 1,500 K, respectively, and the values of rate constants indicating that R_{2a} is declined and the R_{2b} is enlarged with the temperature increasing. The similarly conclusion can be obtained for the reactions R_1 and R_3.

Because of the experimental knowledge of the kinetic nature of the reactions only in the limited temperature, so we hope that our present study may provide useful information for future laboratory investigations. In order to offer further information concerning reactions R_1, R_2 and R_3, the three-parameter fits for the CVT/SCT rate constants of the title reactions in the temperature range 200–1,500 K are performed and expressions are given as follows: (in unit of cm^3 $molecule^{-1}$ s^{-1})

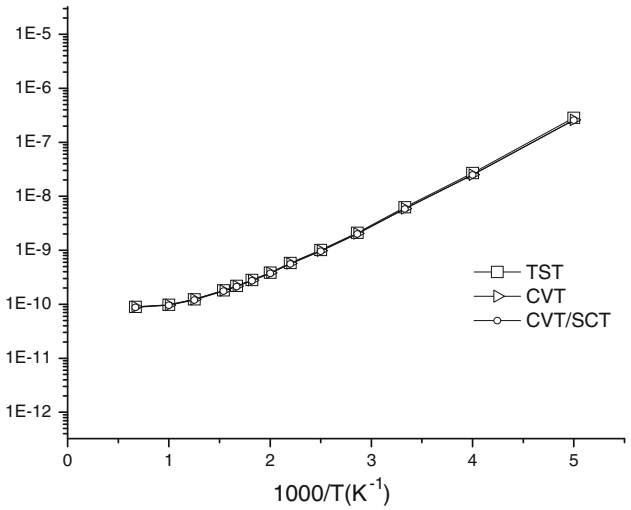

Fig. 6 The TST, CVT and CVT/SCT rate constants calculated at the MC-QCISD//MP2/6-31+G(d,p) level vs. 1,000/*T* between 200 and 1,500 K for the reaction channel $CF_3CH_2CH_2F + Cl \rightarrow CF_3CHOCH_2F + HCl$

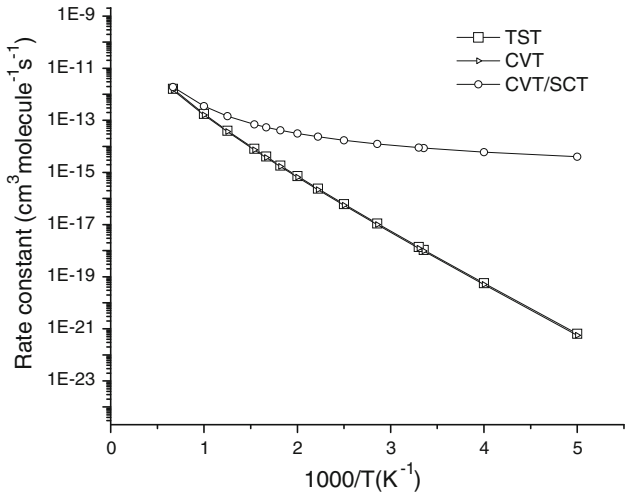

Fig. 7 The TST, CVT and CVT/SCT rate constants calculated at the MC-QCISD//MP2/6-31+G(d,p) level vs. 1,000/T between 200 and 1,500 K for the reaction channel $CF_3CH_2CHF_2 + Cl \rightarrow CF_3CH_2OCF_2 + HCl$

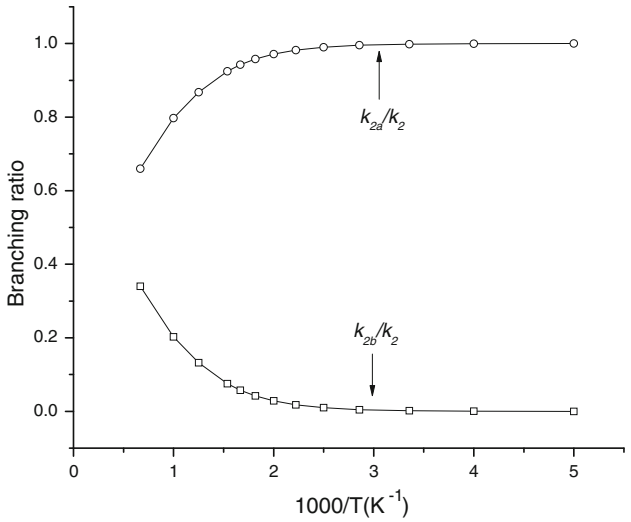

Fig. 8 The branching ratio for R_2 vs. 1,000/T between 200 and 1,500 K at the MC-QCISD//MP2/6-31+G(d,p) level

$$k_1 = 6.99 \times 10^{-16} T^{2.06} \exp(-991.1/T)$$

$$k_2 = 8.38 \times 10^{-18} T^{2.62} \exp(-2981.1/T)$$

$$k_3 = 2.55 \times 10^{-26} T^{4.30} \exp(1059.2/T)$$

4 Conclusions

In the present paper, an ab initio direct dynamics theory have been carried out for investigating the title reactions of $Cl + CF_3CH_2OCH_3$, $Cl + CF_3CH_2OCH_2F$ and $Cl + CF_3CH_2OCH_3$. The potential energy surface information is obtained at the MP2/6-31+G(d,p) level and the higher-level energies for the stationary points and a few extra points along the MEP are calculated by the MC-QCISD method. The bond dissociation energies are also calculated at the same level, and the values of theoretical calculation are in good agreement with the corresponding experimental value. The theoretical CVT/SCT rate constants for each H-abstraction reaction channels are calculated in the temperature range 200–1,500 K, and the value of R_{2a} is the largest one. The rate constants k_1 and k_3 we obtained are in good agreement with the experimental value.

Acknowledgments The authors thank Professor Donald G. Truhlar for providing POLYRATE 9.1 program. This work is supported by the National Natural Science Foundation of China (50743013, 20973049), the Foundation for University Key Teacher by the Department of Education of Heilongjiang Province (1152G010), the SF for leading experts in academe of Harbin of China (2007RFXXG027), the SF for Postdoctoral of Heilongjiang province of China (LBH-Q07058), and Natural Science Foundation of Heilongjiang Province (B200605), The Foundation of Graduate Innovation of the Education Department of Heilongjiang province (YJSCX2009-055HLJ).

References

1. World Meteorological Organization (WMO) (1994) Scientific assessment of ozone depletion. Report No. 37, Geneva, WMO
2. Wallington TJ, Schneider WF, Sehested J, Bilde M, Platz J, Nielsen OJ, Christensen LK, Molina MJ, Molina LT, Wooldridge PWJ (1997) Phys Chem A. 101:8264
3. DeMore WB, Sander SP, Golden DM, Hampson RF, Kurylo MJ, Howard CJ, Ravishankara AR, Kolb CE, Molina MJ (1997) Chemical kinetics and photochemical data for use in stratospheric. JPL Publication 97:4
4. Oyaro N, Sellevag SR, Nielsen CJJ (2005) Phys Chem A 109:337
5. Kyriakos GK, Yannis GL, Panos PJ (1998) Phys Chem. A 102:8620–8625
6. Beach SD, Hickson KM, Smith IWM, Tuckett RP (2001) Phys Chem Chem Phys 3:3064
7. Wallington TJ, Hurley MD, Fedotov V, Morrell C, Hancock GJ (2002) Phys Chem A 106:8391
8. Hickson KM, Smith IWM (2001) Int J Chem Kinet 33:165
9. Yang L, Liu JY, Wang L, He HQ, Wang Y, Li ZSJ (2008) Comput Chem 29:550–561
10. Truhlar DG (1995) In: Heidrich D (ed) The reaction path in chemistry: current approaches and perspectives. Kluwer, Dordrecht, p 229
11. Truhlar DG, Garrett BC, Klippenstein SJJ (1996) Phys Chem 100:12771
12. Hu WP, Truhlar DGJ (1996) Am Chem Soc 118:860
13. Corchado JC, Chuang YY, Fast PL, Villa J, Hu WP, Liu YP, Lynch GC, Nguyen KA, Jackels CF, Melissas VS, Lynch BJ, Rossi I, Coitino EL, Ramos AF, Pu J, Albu TV (2002) POLYRATE version 9.1. Department of Chemistry and Supercomputer Institute, University of Minnesota, Minneapolis
14. Truhlar DG, Isaacson AD, Garrett BC (1985) In: Baer M (ed) The theory of chemical reaction dynamics, vol 4. CRC Press, Boca Raton, p 65
15. Truhlar DG, Garrett BC (1980) Acc Chem Res 13:440

16. Duncan WT, Truong TNJ (1995) Chem Phys 103:9642
17. Frisch MJ, Head-Gordon M, Pople JA (1990) Chem Phys Lett 166:275
18. Head-Gordon M, Pople JA, Frisch MJ (1988) Chem Phys Lett 153:503
19. Zhang H, Liu JY, Li ZS, Sheng L, Wu JY, Sun CC (2005) Chem Phys Lett 405:240–245
20. Yu X, Li SM, Xu ZF, Li ZS, Sun CCJ (2001) Phys. Chem. A 105:7072–7078
21. Zhang QZ, Wang SK, Gu YSJ (2002) Phys Chem. A 106:3796–3803
22. Li QS, Luo Q (2003) J Phys Chem. A 107:10435–10440
23. Yu YM, Feng SY, Feng DC (2005) J Phys Chem. A 109:3663–3668
24. Zhang QZ, Gu YS, Wang SKJ (2003) Phys Chem. A 107:8295–8301
25. Fast PL, Truhlar DGJ (2000) Phys Chem A 104:6111
26. Frisch MJ, Trucks GW, Schlegel HB, Scuseria GE, Robb MA, Cheeseman JR, Montgomery JAJ, Vreven T, Kudin KN, Burant JC, Millam JM, Iyengar SS, Tomasi J, Barone V, Mennucci B, Cossi M, Scalmani G, Rega N, Petersson GA, Nakatsuji H, Hada M, Ehara M, Toyota K, Fukuda R, Hasegawa J, Ishida M, Nakajima T, Honda Y, Kitao O, Nakai H, Klene M, Li X, Knox JE, Hratchian HP, Cross JB, Adamo C, Jaramillo J, Gomperts R, Stratmann RE, Yazyev O, Austin AJ, Cammi R, Pomelli C, Ochterski JW, Ayala PY, Morokuma K, Voth GA, Salvador P, Dannenberg JJ, Zakrzewski VG, Dapprich S, Daniels AD, Strain MC, Farkas O, Malick DK, Rabuck AD, Raghavachari K, Foresman JB, Ortiz JV, Cui Q, Baboul AG, Clifford S, Cioslowski J, Stefanov BB, Liu G, Liashenko A, Piskorz P, Komaromi I, Martin RL, Fox DJ, Keith T, Al-Laham MA, Peng CY, Nanayakkara A, Challacombe M, Gill PMW, Johnson B, Chen W, Wong MW, Gonzalez C, Pople JA (2003) GAUSSIAN03 program package. Pittsburgh, Gaussian
27. Lu DH, Truong TN, Melissas VS, Lynch GC, Liu YP, Grarrett BC, Steckler R, Issacson AD, Rai SN, Hancock GC, Lauderdale JG, Joseph T, Truhlar DG (1992) Comput Phys Commun 71:235
28. Garrett BC, Truhlar DG, Grev RS, Magnuson AWJ (1980) Phys Chem 84:1730
29. Liu Y-P, Lynch GC, Truong TN, Lu D-H, Truhlar DG, Garrett BCJ (1993) Am Chem Soc 115:2408
30. Truhlar DGJ (1991) Comput Chem 12:266
31. Chuang YY, Truhlar DGJ (2000) Chem Phys 112:1221
32. Rayez MT, Rayez JCJ (1994) Phys Chem 98:11342
33. Harmony MD, Laurie VW, Ramsay RL, Lovas FJ, Lafferty WJ, Maki AGJ (1979) Phys Chem 8:619
34. Shimanouchi T (1972) Tables of molecular vibrational frequencies consolidated, vol I. National Bureau of Standards, US GPO, Washington, DC, pp 1–160
35. Shimanouchi T (1972) Tables of molecular vibrational frequencies consolidated, volume II. J Phys Chem Ref Data 6(3):993–1102
36. Chase MW, Davies CA (1985) Janaf thermochemical tables, 3rd edn. Ref Data, 14,1